

# Arresting Rainfall-induced Red Soil Runoff in a Farmland by Inhibitory Adaptation Measures

K. Araki<sup>1</sup>, N. Yasufuku<sup>2</sup>, K. Iwami<sup>3</sup>, K. Okumura<sup>4</sup>, K. Omine<sup>5</sup>, and K. Vilayvong<sup>6</sup>

Graduate School, Department of Interdisciplinary Research, University of Yamanashi, Kofu, Yamanashi, Japan  
 Kyushu University, Fukuoka, Japan  
 Nagasaki University, Nagasaki, Japan  
 E-mail: karaki@yamanashi.ac.jp

**ABSTRACT:** Climate change-induced red soil erosion in Okinawa of Japan has become widely recognized due to the increased frequencies of heavy rainfall. Approximately 85% of runoff from farmland is accounted as a source of the red soil erosion. In this study, field experimental plots were conducted in Ginoza village in Okinawa to investigate the effectiveness of potential adaptation measures in arresting the red soil erosion. A physical model for estimating a sediment volume of soil erosion was derived based on grain size distribution. The maximum particle sizes were derived as a function of rainfall intensity, initial soil conditions and strength parameters of the surface soil. The measured maximum particle sizes of the discharged red soil were agreed well with the model results and could offer the basis for determining an appropriate method of adaptation based on geotechnical aspect.

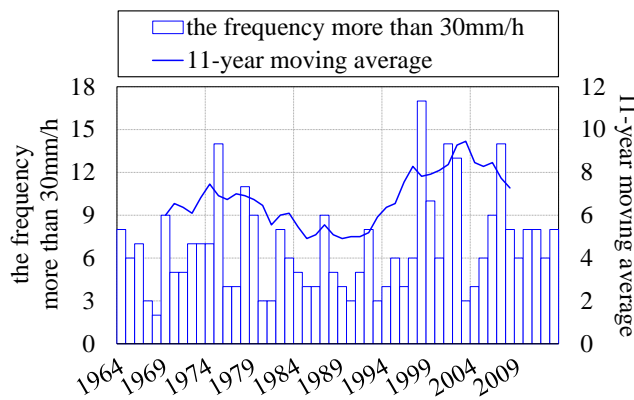
**KEYWORDS:** Red soil runoff, Climate change, Heavy rainfall, Adaptation measure

## 1. INTRODUCTION

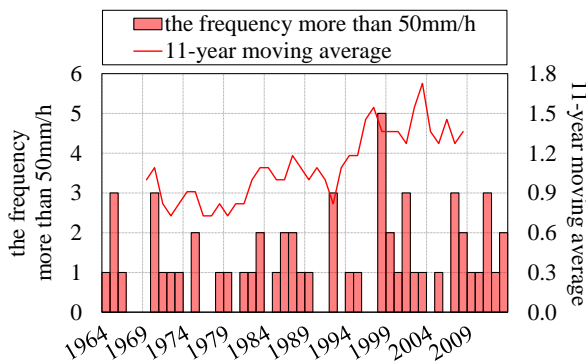
Past 30-year records of the global warming in Okinawa prefecture of Japan show the increase of the frequency of annual heavy rainfall (Okumura et al., 2012; Araki et al., 2014; JMA, 2015; Yasufuku et al., 2015). The rainfall of intensity exceeding 30 mm/h or heavy rainfall (defined by the Japan Meteorological Agency) has been increased (Figure 1). As a result, occurrences of rainfall-induced landslides and floods are widely observed and created a negative impact on tourism, aquatic ecosystem and marine products.

A study conducted by the Prefectural Government of Okinawa in 2015 indicates a clear correlation between rainfall intensity, rainfall patterns and soil outflow. Heavy rainfall associated with climate change increases the volume of red soil runoff and sediments. Approximately, 85% of such runoff comes from farmland (Figure 2). Red soil erosion affects Mozuku (*Cladosiphon Okamuraanus*), highly popular edible seaweed farmed in Okinawa. The Mozuku has been seriously damaged by the red soil runoff in Ginoza Village due to settling of the red soil sediments on the seaweed (Kanda, 2015). Moreover, water turbidity in a coastal area in Okinawa correlates strongly with the frequency of typhoon. Therefore, sustainable adaptation measures for inhibiting the red soil erosion are necessary to minimize the adverse effect on environment.

In this study, series of field experiments in Ginoza village in Matsuda district of Okinawa were arranged and investigated to study physical and mechanical characteristics of the Kunigami red soil erosion using different adaptation measures. Grain size distributions of the discharged sediments are used to characterize the effectiveness of appropriate adaptation measures. The adaptation measures are selected based on the practicality and ease of implementation and application under consideration of cost effectiveness, material availability, sustainability and environment (Okumura et al., 2012; Araki et al., 2013). Effectiveness of the adaptation measures is evaluated by the inhibitory effect of the measures against red soil runoff. The investigation was equipped with the aid of weather station and an online real time monitoring system as a tool for remotely sharing information and data on the status of rainfall, soil and soil runoff and adaptation measures in the field.



(a) Frequency of rainfall exceeding 30 mm/h



(b) Frequency of rainfall exceeding 50 mm/h

Figure 1 Trend of the frequency of heavy rainfall

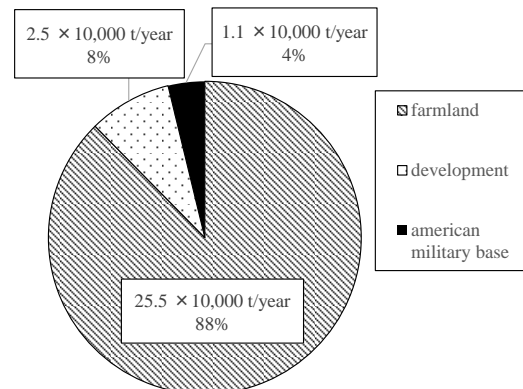


Figure 2 The statistics of the red soil runoff in Okinawa in 2011

**2. PHYSICAL PROPERTIES OF KUNIGAMI SOIL**

Kunigami soil is a typical red soil distributed in the north central Okinawa and the surrounding islands. It is reddish to yellowish in color, highly acidic and derived from slate and Kunigami gravels. Figure 3 shows the grain size distribution of the soil and its fitting grain size distribution curve derived from regression analysis using a logarithmic normal distribution function. The simulated result matched the trend of the experimental data. The correlation coefficient between experimental data and simulation results was 0.997. Table 1 shows the particle density and plasticity index and soil classification of the Kunigami soil collected from Ginoza village of Matsuda district in Okinawa.

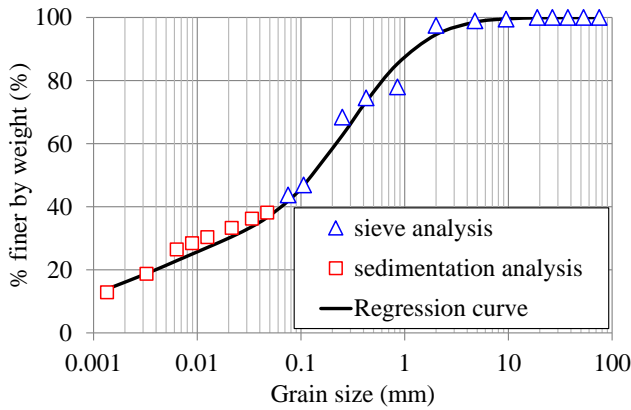


Figure 3 Grain size distribution curve of the Kunigami soil

Table 1 Physical properties of the Kunigami soil

Soil particle density	Liquid limit	Plastic limit	Plasticity index
$\rho_s$	$w_L$	$w_P$	$I_P$
( $g/cm^3$ )	(%)	(%)	(-)
2.67	31.3	19.5	11.8

**3. ARTIFICIAL SEDIMENT RUNOFF EXPERIMENTS**

**3.1 Rainfall experiment set-up**

Figure 4 shows a schematic drawing of the indoor rainfall experiment. Dimension of a soil container was 88.5 cm x 25 cm x 8 cm with a closed bottom and sides to set the boundary condition as no drainage.

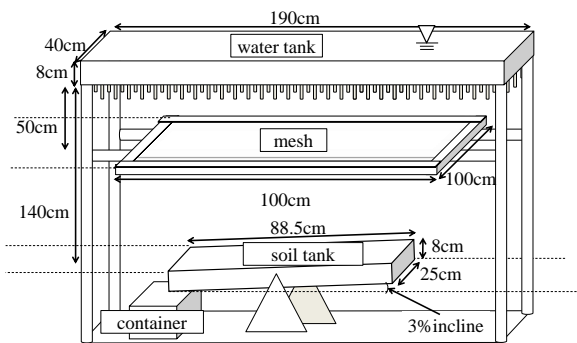


Figure 4 Configuration of rainfall experiment

A rainfall simulator was constructed with the use of hypodermic needles (1.25 mm outer diameter). The needles were attached to a water tank of 190 cm x 40 cm x 8 cm. The tank was connected to a water inlet using a hose and flow volume was monitored by manual reading flow meter (in L/min unit) attached in the middle of the hose. The raindrop was allowed to fall from the tip of the needles at a height of 1.4 m to soil surface in the middle of the soil container. To reduce

effect of drop-formed crater on the soil surface, a screen net made of metal mesh of an opening size of 0.5 mm was placed at 50 cm below the tip of the needles.

Figure 5 shows the calibration of precipitation in mm using the rainfall simulator. 60-minute precipitation was recorded. The calibration was carried out seven times. Result suggested that the precipitation recorded at 10-minute interval increased linearly with the accumulated precipitation. Maximum rainfall precipitation capacity the tank can produce was 35-45 mm, equivalent to rainfall intensity of 35-45 mm/h. Rainfall intensity exceeding 30 mm/h is classified as an intense rainfall category as defined by the Japanese Meteorological Agency.

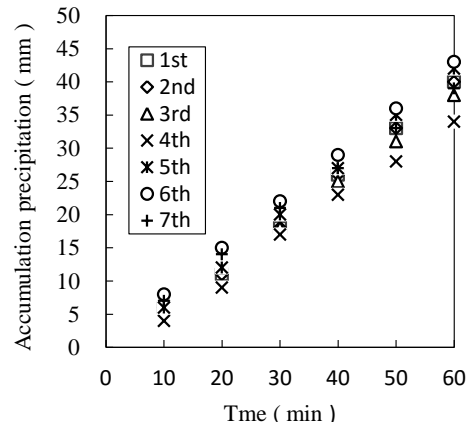


Figure 5 Calibration of the artificial rainfall in the laboratory

**3.2 Experimental method**

Rainfall experiments were carried by allowing the simulated rainfall dropped onto the soil surface inclined at 3% slope. 60-minute rainfall period of intensity of 35-45 mm/h was conducted. It was carried out on six conditions under different initial water contents and initial dry densities. Table 2 shows the soil conditions prepared for the rainfall experiments. Figure 6 the compaction curve and relationship between compaction energy-dry density-water content of the red soil. Surface runoff was measured by using a water container placed at the outlet of the soil container. Soil loss or sediment concentration was calculated by multiplying collected volume of runoff with mass of dry soil present in the sampling of the runoff. The dry mass was calculated using three sampling volume of 100 ml of the runoff and dried in oven at a temperature of 105 °C. Particle size of the eroded soil was obtained using a particle size laser analyzer device.

Table 2 Soil conditions for rainfall experiments

	Case1	Case2	Case3	Case4	Case5	Case6
initial water content (%)	16.11	15.24	1.79	0.50	1.22	8.48
initial dry density ( $g/cm^3$ )	1.73	1.87	1.35	1.48	1.66	1.65
initial degrees of saturation (%)	79.76	96.56	4.94	1.69	5.44	37.04
initial void ratio (%)	0.55	0.43	0.97	0.80	0.61	0.62
the amount of surface water (l)	6.06	6.51	2.26	4.50	5.39	6.35
the amount of red soil runoff (g)	48.30	65.65	7.50	25.73	17.97	22.78

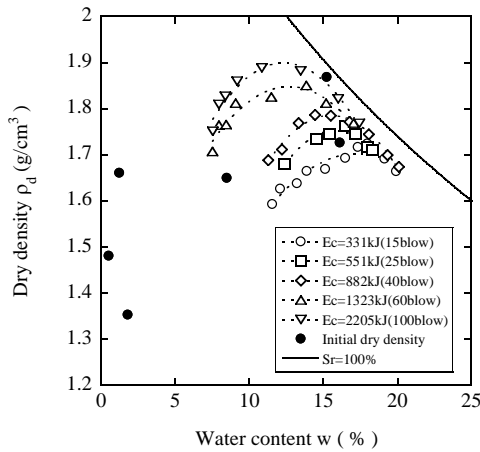


Figure 6 The compaction curve of the red soil

**3.3 Comparison of red soil runoff results**

Figure 7 shows the relationship between soil loss and runoff for all initial conditions in the rainfall experiments for 60-minute rainfall under the intensity of 35-45 mm/h. This result indicated that the initial conditions affected soil loss and runoff behavior. At the higher initial water content and higher density (case 2), rainfall simulator produced maximum soil runoff and soil loss. This was due to wetting front and low permeability at the higher dry density. On the other hand, minimum runoff and soil loss were occurred in case 3 because loose soil condition (low dry density) at dried soil state (low water content) allowed higher water infiltration.

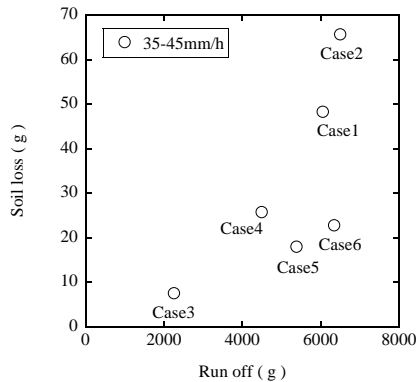


Figure 7 Relationship between soil loss and runoff

Figure 8 shows the comparison results for runoff and soil loss at the similar initial dry density (1.65 g/cm³) and varying initial water contents for case 1, case 5 and case 6. The results indicated that with similar dry densities, runoff (measured in g) in all cases showed similar mass collected.

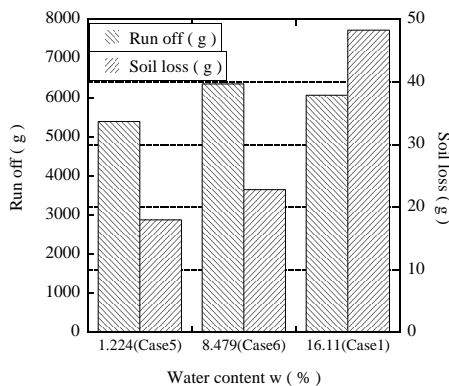
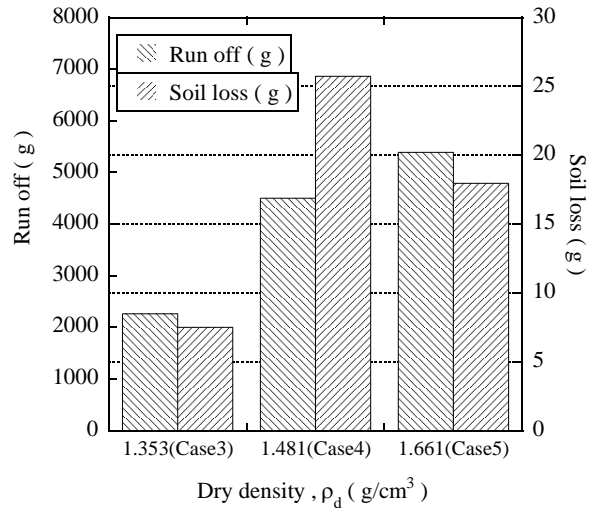


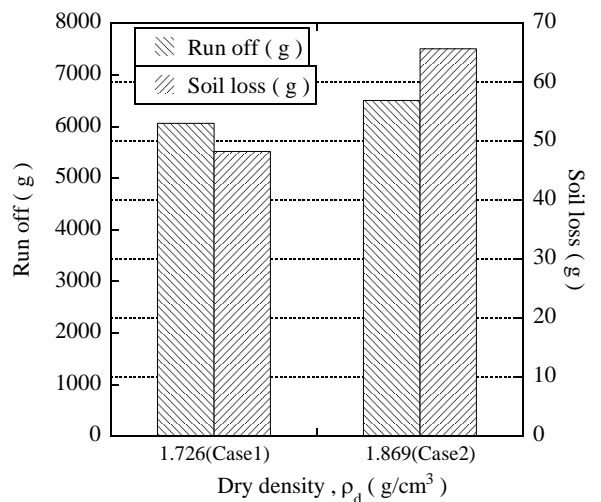
Figure 8 Soil loss and runoff at similar initial dry density

However, it was evident that the large variation of soil loss in all cases was observed. This was due to the variation in initial moisture contents and increase in water content. Maximum soil loss was observed in case 1, whereas case 5 produced the minimum soil loss. In addition, it was expected that the surface infiltration contributed to the disparity and different soil textures derived from the effect of soil compaction were also expected.

Figure 9 shows comparison results of runoff and soil loss at similar initial water contents and varying dry densities. Figure 9(a) shows the results at the similar initial water content (about 1%) for case 3, case 4 and case 5 and Figure 9(b) shows the results at similar initial water content (about 15%) for case 1 and case 2. Results in Figure 9(a) showed the large variation in runoff and soil loss collected and the results did not show similar trending for the runoff and soil loss, where maximum runoff and soil loss were produced in case 5 and case 4, respectively. This indicated that at short heavy rainfall, soil at initial dry state did not increase soil loss with respect to the increase in moisture content due to difference in initial dry density. However, at higher initial wet condition as case 1 and 2 (Figure 9b) showed slightly difference in runoff and soil loss. It is suspected that at high dry density with high water content, soil textures were similar and it was difficult for rainfall to percolate into the soil resulting in similar runoff and soil loss during the short duration of the applied rainfall.



(a) at initial water content at 1%



(b) at initial water content at 15%

Figure 9 Soil loss and runoff at similar initial water contents

**3.4 Comparison of the particle sizes of sediment in the outflow runoff**

Figure 10 shows the grain size distributions of the red soil before and after rainfall experiments. Particle sizes of the eroded soils for the six cases in the experiments were found to be different. However, there were not significant differences in all eroded soils. It was found that the biggest particle size of the eroded soil was approximately 0.02 mm in diameter, whereas the biggest particle size of the soil before experiment was approximately 10 mm in diameter. Furthermore, maximum particle size 0.02 mm of the outflow soil was corresponding to percent finer of the local soil at approximately 30%. As a result, the quantity of soil loss was determined to be approximately 30% of the mass of the soil before experiment.

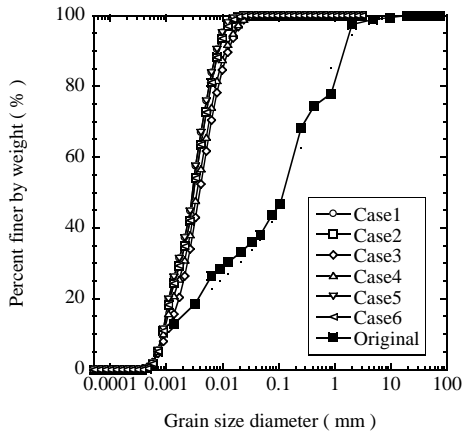


Figure 10 Grain size distribution of the eroded soil before and after rainfall experiment

**4. FIELD TEST OVERVIEW**

**4.1 Field Experiment Overview**

Experimental site was prepared and divided into seven erosion plots of similar size (1.5 m width x 6.0 m length) inclined at 3% slope using a mini backhoe as shown in Figure 11. Several inhibitory materials against soil erosion were applied in each plot with different arrangements. Abandoned farmland, biological soil crust (BSC) and compost were applied to the whole area of each plot. Sand mats, grass mats and green belts were applied to the outlet section. Plates were installed 10 cm above soil surface at top side, right side and left side to prevent water inflow and outflow from the plots. In the discharged outlet of each plot, three plastic containers were installed in a cascading manner to collect turbid runoff as shown in Figure 12. Sampling of the runoff was conducted monthly as to avoid the generation of fungi and algae in the collected runoff in the containers.

**4.2 Adaptation Measures**

There are some studies reported on the measuring amount of the red soil runoff from a farmland (Ikeda, 2004; Shiono et al., 2004). However, criteria for selecting the appropriate adaptation methods are not broadly available. In this study, seven adaptation measures were selected under consideration of practicality, material availability, low cost and minimal labor.

Figure 13 shows the adaptation measures set up in the field experimental plots. The properties of these measures are listed in details below.

**(a) Abandoned area**

Number of abandoned areas in the vicinity is rising due to shortage of farming laborers and increasing number of aged farmers. It is therefore important to conduct a study to link abandoned areas to soil runoff as a control measure.

**(b) Biological Soil Crust (BSC) area**

Biological Soil Crust (BSC) is a microorganism-induced soil crust formed by fungi and algae on the soil surface. Soil detachment and sediment runoff are expected to reduce because bonded soil particles can withstand the shearing from runoff flow. The BSC is considered as an effective measure against soil erosion as other measures using vegetation covers (i.e. sugar cane).

**(c) Compost area**

Compost materials improve the soil aggregation by binding soil particles together as an aggregate. However, the inhibitory effect of the aggregation on soil runoff is expected in the compost areas. 90 kg of compost was mixed into the entire 10 kg/m<sup>2</sup> area of an erosion plot.

**(d) Bare land**

Bare land plot was prepared for comparing with other adaptation measures. Most red soil runoff is initially occurred in bare land area and red soil erosion is expected to reduce until vegetative covers and protective plants are formed.

**(e) Sand mats**

60 kg of coral sand was applied to the outlet section at the toe of the 3% slope. Approximately, 80 kg/m<sup>2</sup> of the sand was put in a net-typed permeable bag to prevent the escape of the sand grains from soil detachment and surface runoff due to rainfall.

**(f) Grass mats**

Grass mats using grass straws are commonly and widely used as a control measure in the surrounding areas. Grass mats were placed at the outlet section at the toe of 3% slope, similar to that of the sand mats.

**(g) Green belts**

Green belts or Vertiver grass (*Vetiveria zizanioides*) is a typical local plant. The root of the plant can penetrate the subsurface soil and the root density and stems can minimize the soil erosion. Figure 11 shows a view of the field experimental site and Figure 12 shows the outlined arrangements of the field experiments.



Figure 11 Tested erosion plots in the experimental site

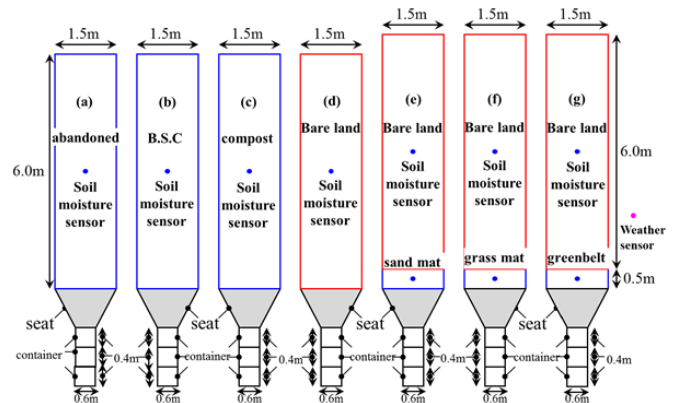


Figure 12 Outline of the field test

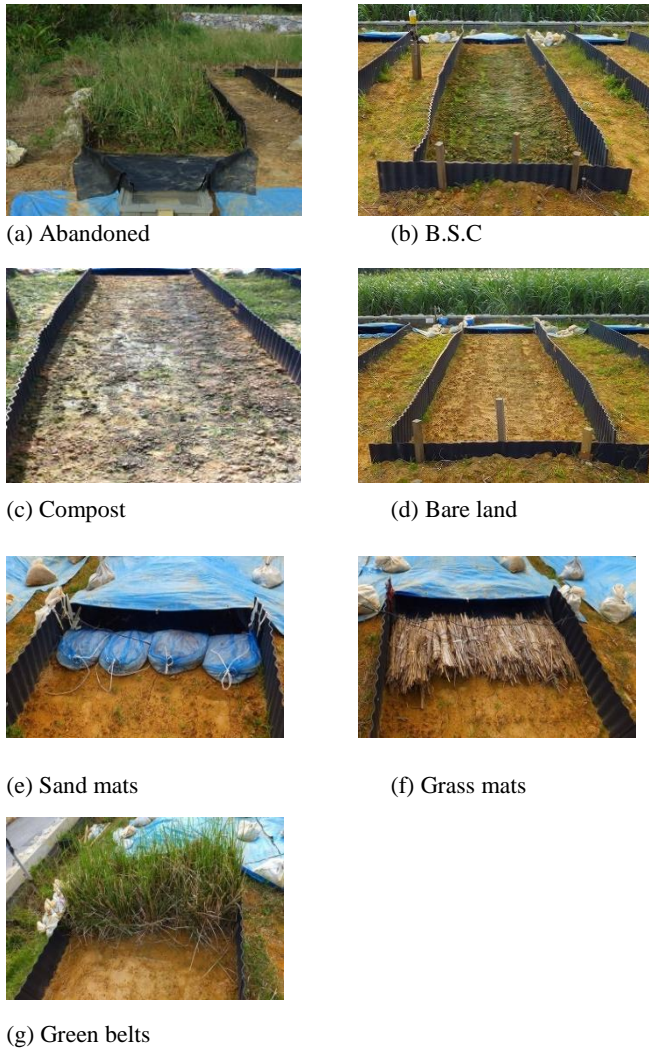


Figure 13 Adaptation measures against soil erosion and runoff

**4.3 Real-Time Monitoring System for Remote Site**

In field experiments, an online and real-time monitoring system for remotely acquiring the weather information such as rainfall, temperature, atmospheric pressure, humidity, wind velocity and soil volumetric water content. The data are remotely shared and used by the Okinawa prefectural government, the local Ginoza village government and farmers. The system can inform the users about the situation of sediment discharge and soil condition by sending alert signals. The alert signals are marked by monitoring the liquid and plastic limits. This method can increase the awareness of the formers and users about sediment discharge from farmland in a timely manner.

Weather station and soil moisture sensors were installed as shown in Figure 12. 10 numbers of soil moisture sensors from Decagon (EC-5) were installed at 5 cm depth below the soil surface. Figure 14 shows the system setup. Figure 15 shows the monitored rainfall and volumetric water contents from May 24 2012 to June 22, 2012. Figure 15 also indicates that the volumetric water content started to rise immediately after rainfall. It was observed that the volumetric water content of the division plot covered with BSC was about 10% higher than that of bare land. This was due to the restraining effect of the BSC from moisture evaporation from the soil surface. The moisture ratio in the division plot with compost changed relatively quickly as a result of soil aggregation.

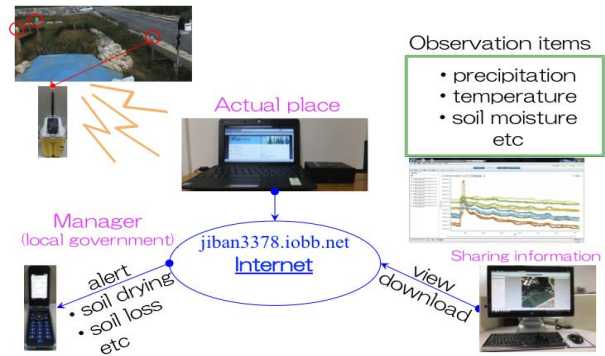


Figure 14 Real-time monitoring system

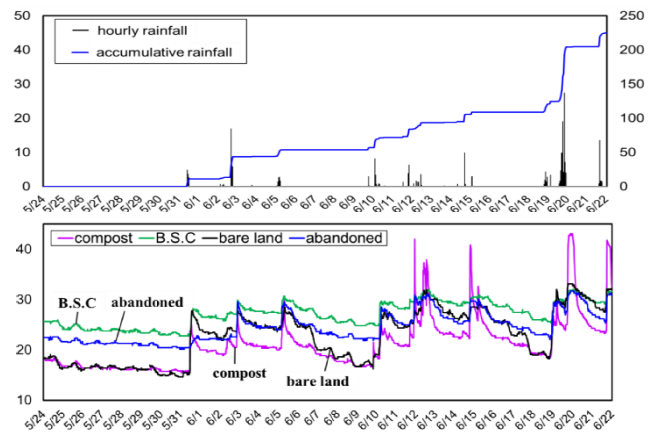


Figure 15 Observation data for rainfall and soil conditions

**5. INHIBITORY EFFECT OF SOIL RUNOFF DUE TO ADAPTATION MEASURES**

Figure 16 shows the amount of the accumulative soil runoff from December 26, 2011 to June 23, 2013. Figure 17 shows the daily and accumulative rainfall corresponding to Figure 16 with minimum turbid water outflow amount from 2011 to 2013. Rainfall data was obtained from Higashi Village, the nearest meteorological station to the field experiments. In soil erosion study, short rainfall is an important factor. Instead, in this study, daily rainfall was considered because the observation period exceeded 4 weeks. It was useful to conduct monitoring and measurement for a period of 16 months as to evaluate both the short-term and long-term effects of individual adaptation so that basic baseline data can be established. Dry weight of soil runoff sediment was determined from the volume and concentration of turbid water. Concentration was determined by sampling the turbid runoff water after stirring the discharge runoff stored in the plastic containers. The six divisions, except abandoned plot, were sampled once a month. Figures 16 and 17 show the trend of rainfall; the higher the rainfall increases, the greater the amount of accumulative soil runoff attained.

The amount of minimum turbid water outflow in Figure 17(b) shows the similar trend with the accumulative rainfall pattern in Figure 17(a). The red soil runoff from the bare land plot exceeded that of other division plots especially during the period from April to October 2012. After November 2012, the gradients of the graphs became smaller except for that of the grass mats. However, more detailed field investigations are needed to determine the differences. From April 2012, the amount of runoff in the BSC plot was increased. It was expected that effectiveness of the applied

BSC limited was about 4 months. Rainfall exceeding 30 mm/h was recorded 5 times during this period. Therefore, the data was one of the indices for clarifying the application limit. In the month in which rainfall exceeding 250 mm/day was recorded, the amount of soil runoff from the grass mats and compost plots exceeded that of other periods as the trends were clearly seen. In contrast, the amount of soil runoff from plots using sand mat and green belts was not so significant during the same period. This was due to the reduction in permeability of soil surface resulting in higher volume of soil runoff

in the sand mat and green belt division plots during heavy rainfall. From 16<sup>th</sup> month onward, the green belts reduced soil runoff effectively and this division plot was less susceptible to precipitation induced erosion. As a result, the green belt was proven to be useful as the grass mat. In contrast, the amount of soil runoff in the abandoned plot was the second largest until June 2012 and was reduced drastically from June 2012 due to the presence of vegetation covers that occurred locally and naturally.

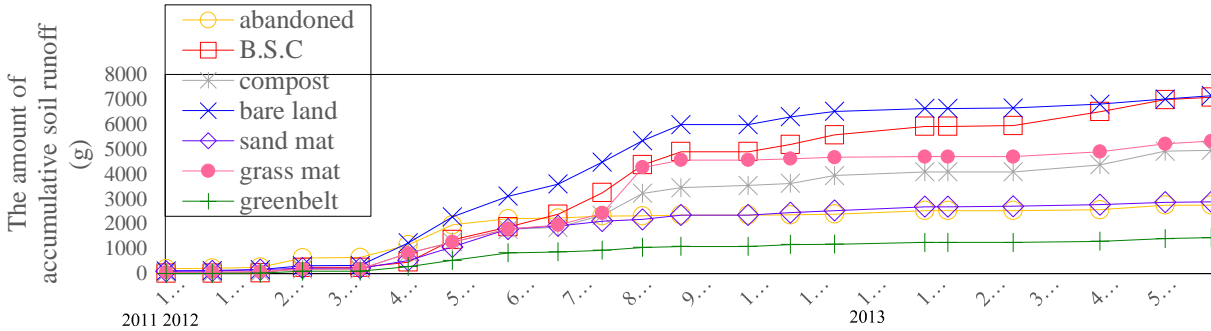
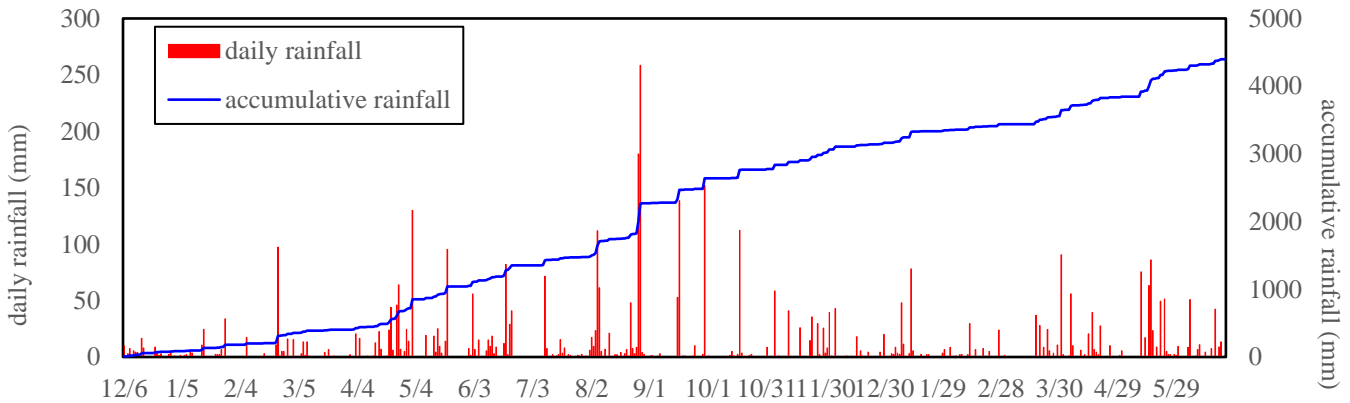
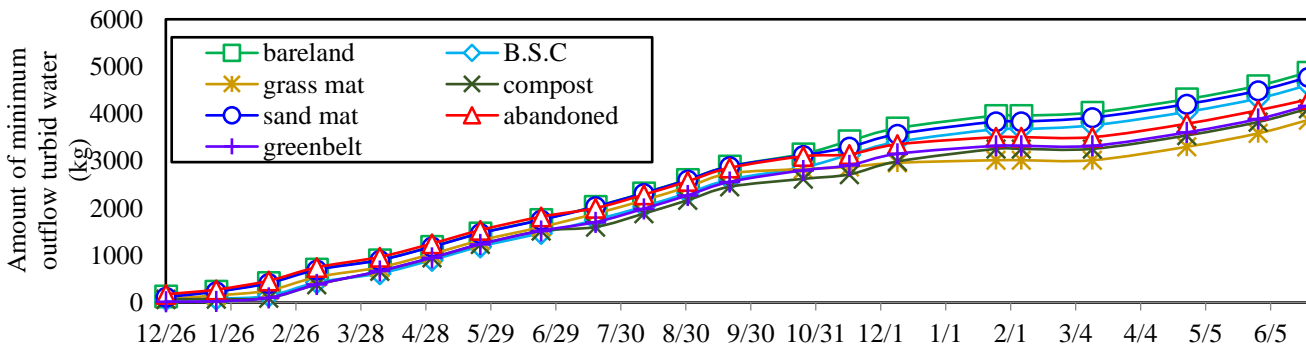


Figure 16 Results of the amount of red soil runoff from 2011 to 2013



(a) Daily and accumulative rainfall from 2011 to 2013



(b) Minimum turbid water outflow from 2011 to 2013

Figure 17 Daily and accumulative rainfall from 2011 to 2013

**6. GRAIN SIZE DISTRIBUTION OF THE DISCHARGED SEDIMENTS**

Sedimentation ponds are widely set up in Okinawa to prevent soil sediment flow out into aquatic system such as rivers and seas. The sedimentation ponds are effective to retain turbid runoff and settle soil particles of the sizes exceeding 0.2 mm in diameter. Thus, it is

important to investigate the grain size distribution of the sediments discharged when different adaptation measures were applied to farmland. In this study, maximum grain size ( $D_{max}$ ) of the discharged soil was used as important information for determining the effectiveness of inhibitory adaptation measures. Figure 18 shows the grain size distribution collected from three containers in each erosion plot.

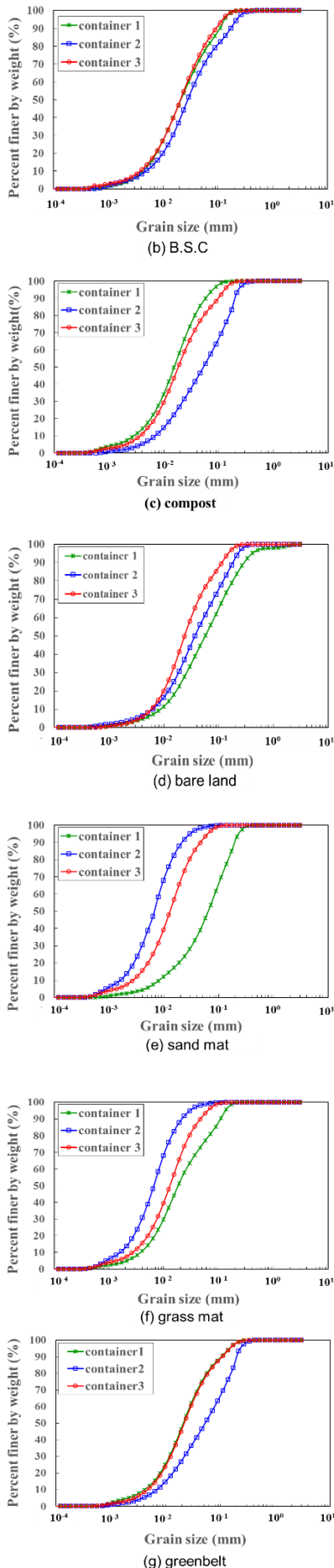


Figure 18 Grain size distributions of the discharged sediments

Table 3 shows the grain size at 50% percent finer ( $D_{50}$ ) and the amount of discharged soil. The  $D_{50}$  in each storage container was computed by regression analysis during measurement period from May 30 to June 23, 2013. Accumulative rainfall exceeding 165.5 mm and rainfall intensity exceeding 30 mm/h, the sizes of discharge sediments were not recorded during this measurement period. Thus, it will be important in the future work that the grain size distribution of red soil runoff during heavy rainfall be investigated.

Table 3 Properties of the discharged sediment

measure	$D_{max}$	$D_{50}$	$U_c$	$U_c'$	the amount of discharged soil
-	$\mu m$	$\mu m$	-	-	g
Greenbelt	559.5	24.6	6.0	0.97	38.9
Grass mat	112.6	14.7	6.4	0.97	112.8
Sand mat	575.4	30.4	6.2	0.98	22.3
Bare land	544.8	37.2	8.4	0.95	132.2
Compost	583	21.4	6.4	0.97	38.9
B.S.C	418.6	18.7	6.1	0.98	93.8
abandoned	-	-	-	-	0

$$D_{50} = (D_{50①} \times M_① + D_{50②} \times M_② + D_{50③} \times M_③) / (M_① + M_② + M_③)$$

M: dry weight (g)

①~③: container 1~container 3

Figure 19 shows the average monthly rainfall in Higashi village, the nearest meteorological station to the field experiment site. The rainfall was used as a standard rainfall during measurement for a period from 1981-2010. Grain size distribution in the abandoned area was not shown because no occurrence of red soil runoff was observed. This indicated that no clear trend existed between grain size distributions in the storage container 1 to the storage container 3. The  $D_{50}$  on bare land exceeded that of any other erosion plot. Therefore, it was concluded that the discharged soil particles could be smaller by the selected adaptation measures. It was confirmed that 60% of all soil grain sizes presented in the runoff can be occurred during the measurement period. The coefficient of uniformity ( $U_u$ ) and the coefficient of curvature ( $U_c$ ) are showed in Table 3. The  $U_c$  of the field soil in Fig. 3 was higher than that of the  $U_c$  in the discharged soil. This confirmed that the soil particles of the discharged soil were smaller than that of the field soil before experiment.

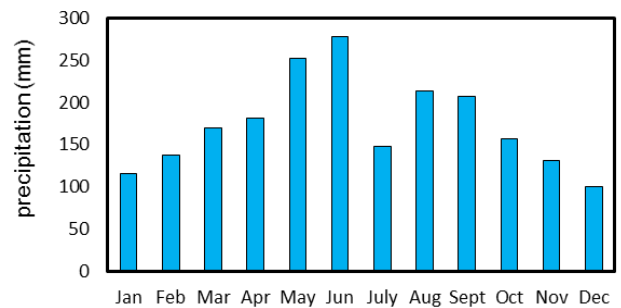


Figure 19 Average monthly rainfall from 1981 to 2010 in the Higashi village

7. ESTIMATION OF OUTFLOW LIMIT PARTICLE SIZE

Araki et al. (2011) proposed an equation for estimating outflow based on limit particle size  $D_{max}$  of a soil. Detailed derivation of the equation was presented in the Appendix A.

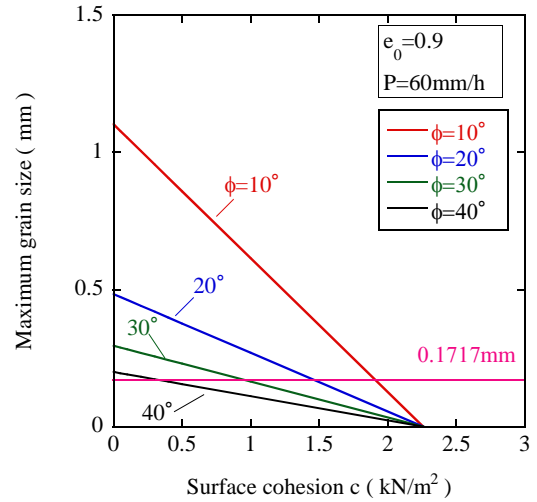
$$D_{max} = \frac{(c - Q\rho_w g \sin \theta) S_r^{-\frac{1}{3}} (\pi/6)^{-\frac{1}{3}} e^{\frac{2}{3}}}{(\rho_s - \rho_w S_r) g (\sin \theta - \cos \theta \tan \varphi)} \quad (1)$$

where  $\theta$  is the average slope angle,  $c$  is the apparent cohesion and  $\phi$  is the soil internal friction angle,  $Q$  is the amount of surface flow volume due to rainfall intensity,  $\rho_s$  is the soil solid density and  $\rho_w$  is the water density,  $S_r$  is the degree of saturation and  $e$  is the initial void ratio. Slope angle  $\theta$  is 3%, corresponding to typical field angle in the area. The initial void ratio of the ground surface was 0.9 under  $S_r = 100\%$ , so  $Q$  was calculated by subtracting the coefficient of permeability from hourly rainfall. Estimated outflow based on limit (maximum) particle grain size versus strength parameters is shown in Figure 20. Note that the maximum grain size was strongly influenced by the internal friction of the soil surface and cohesion. It was found that the soil loss became zero when cohesion exceeded a certain value. When rainfall intensity increased, the surface cohesion also increased and soil runoff reduced. The measured maximum grain size of the red soil was in the range of 0.06–0.3 mm, as depicted in Figure 20. The measured internal soil surface friction angle and the cohesion were 30–40° and 0.2–0.5 kN/m<sup>2</sup>, respectively. The calculated results were fitted with the measured results and the calculated results could serve as a chart for effectively determining an appropriate adaptation method based on a geotechnical point of view. The cohesion,  $c$ , and internal friction angle,  $\phi$ , were derived by a surface shear test conducted by Iwami et al., 2015

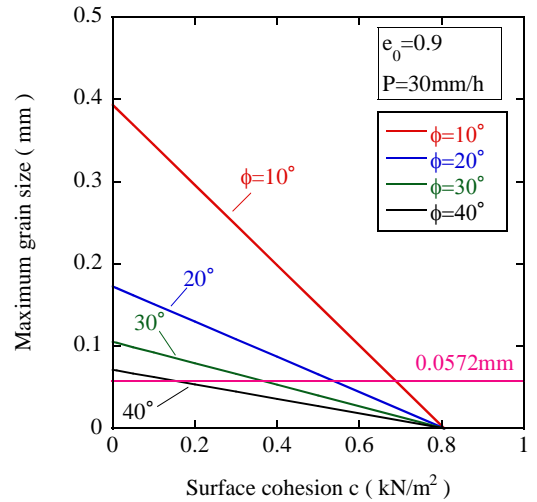
**8. CONCLUSIONS**

This study was carried out experimentally in the field site in Ginoza Village of Okinawa Prefecture. The physically and mechanically based analysis and model were derived based on the data gathered with the aid of an online real time data acquisition and monitoring system. The inhibitory effects of the adaptation measures against red soil runoff using various adaptation measures were assessed. The conclusions are as follows:

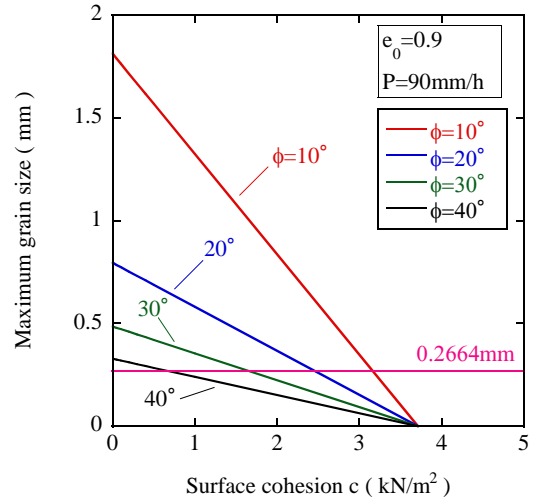
- 1) Artificial rainfall simulation was useful to capture the soil runoff behavior, particularly the characteristics of the grain size distribution of the discharge sediments. The maximum particle size measured from the eroded soil was approximately 0.02 mm. It was suggested that soil loss was approximately 30 % of the particle size distribution curve of the soil before testing.
- 2) Real-time data acquisition and monitoring system using remote communication were a vital tool for recording and sharing data with relevant parties. It provided in-time weather data and status of soil condition efficiently. This system was useful in raising awareness of the concerned parties about status of the red soil sediment discharged from farmland.
- 3) Results recorded during the period of 16-month observation, the erosion plot using green belts (Vertiver grass) was found to be the most effective adaptation measure in arresting the red soil runoff. The erosion plot using sand mat was comparatively less susceptible to rainfall.
- 4) Grain size distribution of the soil discharged from each adaptation plot was assessed and analyzed using the physical parameters  $D_{max}$  and  $D_{50}$ . The grass mat was most effective in controlling a wide range of soil particles from flowing away during the rainfall used in the study.
- 5) The simplified model was proposed for estimating the maximum outflow particle size. The model was a function of rainfall intensity, initial conditions and strength parameters of the soil surface. The model fitted with the estimated maximum grain size of the surface soil. This concluded that the calculated results can be a useful chart for effectively determining the appropriate adaptation measure against rainfall-induced soil erosion based on a geotechnical aspect.



(a) Hourly rainfall P=30 mm



(b) Hourly rainfall P=60 mm



(c) Hourly rainfall P=90 mm

Figure 20 Relationship between the maximum grain size and surface cohesion

**9. ACKNOWLEDGMENTS**

This research was supported by the Environmental Research and Technology Development Fund (S8-2(2)) of the Ministry of the Environment, Japan, and JSPS Kakenhi Grant Number 24760381 and 24656287. The authors are deeply grateful to Ginoza Village in Okinawa Prefecture and to the Tomohiro Fujita of Aoi Consultant Ltd., and Mineto Tomisaka of Nippon Koei Co., Ltd., for their assistance in conducting field experiments.

**10. REFERENCES**

D. Gallipoli, A. Gens, J. Vanet, and E. Romero. (2002). "Role of Degree of Saturation on the Normally Consolidated Behavior of Unsaturated Soils". Proc. 3rd Int. Conf. on Unsaturated Soils, pp. 115-120, 2002.

H. Yamaguchi (2004). "Soil Mechanics". Gihodoshuppan, pp. 38-40, 2004.

Japan Meteorological Agency (2015). Retrived from <http://www.data.jma.go.jp/obd/stats/etrn/index.php?precno=91&blockno=1374&year=&month=&day=&view> [accessed March 22, 2015]

Japan Meteorological Agency (2015). "Rainfall intensity and form" (in Japanese). Retrived from <http://www.jma.go.jp/jma/kishou/known/yougohp/amehyo.html> [accessed March 22, 2015]

K. Araki, K. Okumura, N. Yasufuku, and K. Omine. (2014). "Studies on the inhibitory effect by various adaptation measures for red soil runoff from farmland on field tests, Unsaturated Soils: Research & Applications". The 6<sup>th</sup> Int. Conf. on Unsaturated Soils (UNSAT2014), pp. 1447-1452, 2014.

K. Araki, K. Okumura, N. Yasufuku, and K. Omine. (2013). "A consideration on inhibitory effect of red soil runoff by various adaptation measures on field tests". The 10<sup>th</sup> JGS Symposium on Environmental Geotechnics, pp. 221-226, 2013 (in Japanese).

K. Araki, N. Yasufuku, K. Murayama, K. Omine, and H. Hazarika, (2011). "Modeling for outflow of soil sediments considering grain size distribution". The 2<sup>nd</sup> Japan-Korea Joint Workshop on Unsaturated Soils and Ground, pp. 151-160, 2011.

K. Iwami, K. Araki, N. Yasufuku, R. Ishikura, and H. Hazarika, (2015). "Soil runoff model and its application by focusing soil particle mechanics equilibrium". The JSCE-west annual meeting, No.III-86, 2015 (in Japanese).

K. Okumura, K. Araki, N. Yasufuku, K. Omine, and H. Hazarika. (2012). "Studies on the inhibitory effect of red soil runoff by various adaptation measures on field tests". The Int. Joint Symposium on Urban Geotechnics for Sustainable Development, pp. 140-143, 2012.

N.Yasufuku, K. Araki, K. Omine, K Okumura, K.Iwami. (2015). "Evaluation of inhibitory effect by adaptation measures for red soil runoff from farmland due to heavy rainfall". Journal of Disaster Research, 10(3), 457-466, 2015.

S. Ikeda. (2004). "Watershed management and red clay out suppression system related research and development in Okinawa". AJSCE in 2004 fy "priority research agenda" report, pp. 1-23, 2004 (in Japanese).

T. Shiono, K. Tamashiro, N. Haraguchi, and T. Miyamoto. (2004). "Use of vegetation filter strips for reducing sediment discharge during a rainstorm, participatory strategy for soil and water conservation". Institute of Environmental Rehabilitation and Conservation, pp. 55- 58, 2004.

Y. Kanda (2015). Retrieved from [http://www.inamori.kagoshima-u.ac.jp/kanda/ronbun/activity03\\_02\\_02.html](http://www.inamori.kagoshima-u.ac.jp/kanda/ronbun/activity03_02_02.html) [accessed March 22, 2015]

**Appendix A: Derivation of the Equation (1)**

Bishop's effective stress is defined as follows:

$$\sigma_B' = (\sigma - u_a) + \chi \cdot s_u \tag{A1}$$

where  $\sigma_B$ : Bishop's effective stress,  $\sigma$ : total stress,  $u_a$ : pore air pressure,  $\chi$ : Bishop's parameter, and  $s_u$ : suction.

The following equation is often used, for example, Gallipoli et al. (2002).

$$\chi \cong S_r \tag{A2}$$

Bishop's parameter  $\chi$  is often expressed as follows, for example, Yamaguchi (2004):

$$\chi = \frac{A_w}{A} \tag{A3}$$

where  $A_w$ : area acting of pore water,  $A$ : area acting of total stress.

The volume of water is related using the following equation:

$$V_w = e V_s S_r \tag{A4}$$

where  $V_w$ : volume of water,  $e$ : void ratio,  $V_s$ : volume of soil particles,  $S_r$ : degree of saturation.

Here, considering the isotropy of water, we derived the following equation:

$$A_w = (V_w)^{\frac{2}{3}} \tag{A5}$$

Using (A2), (A3), (A4) and (A5), we derived the following equation:

$$A = (e V_s)^{\frac{2}{3}} S_r^{-\frac{1}{3}} \tag{A6}$$

Figure 21 shows equilibrium for a particle. The sliding condition of the particle is given by the following equation:

$$W \sin \theta + F_q \geq W \cos \theta \tan \phi + F_c \tag{A7}$$

$$F_q = \rho_w g A Q \sin \theta \tag{A8}$$

$$F_c = cA \tag{A9}$$

where  $W$ : own effective weight,  $Q$ : surface water runoff amount,  $\rho_w$ : water density,  $g$ : gravitational acceleration,  $\phi$ : internal friction angle,  $\theta$ : slope gradient,  $c$ : cohesion per contact point.

Here, effective own weight and pore fluid density are expressed as follows:

$$W = (\rho_s - \rho_v) g V_s \tag{A10}$$

$$\rho_v = \frac{W_v}{V_v} \tag{A11}$$

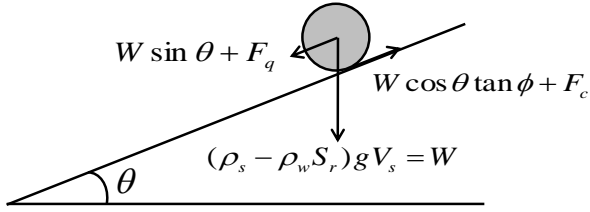


Figure 21 Sliding condition of a particle

where  $\rho_v$ : pore fluid density,  $W_v$ : void weight,  $V_v$ : void volume.

The void weight and void volume are derived as follows:

$$W_v = W_w \quad (A12)$$

$$V_v = e V_s \quad (A13)$$

where  $W_w$ : water weight.

Water weight is expressed as follows:

$$W_w = \rho_w V_w \quad (A14)$$

Using (A10), (A11), (A12), (A13) and (A14), we derived the following equation:

$$W = (\rho_s - \rho_w S_r) g V_s \quad (A15)$$

The spherical particle volume is expressed as follows:

$$V_s = \frac{\pi}{6} D^3 \quad (A16)$$

where  $D$ : the particle diameter.

Using (A6), (A7), (A8), (A9), (A15) and (A16), we derived the following equation:

$$D \leq \frac{(c - Q\rho_w g \sin \theta) S_r^{\frac{1}{3}} (\pi/6)^{-\frac{1}{3}} e^{\frac{2}{3}}}{(\rho_s - \rho_w S_r) g (\sin \theta - \cos \theta \tan \phi)} \quad (A17)$$

The maximum diameter of a sliding particle is written as follows:

$$D_{\max} = \frac{(c - Q\rho_w g \sin \theta) S_r^{\frac{1}{3}} (\pi/6)^{-\frac{1}{3}} e^{\frac{2}{3}}}{(\rho_s - \rho_w S_r) g (\sin \theta - \cos \theta \tan \phi)} \quad (A18)$$

where  $D_{\max}$ : the maximum diameter of a sliding particle.